Ultrafast molecular dissociation induced by intermolecular Coulombic decay in water clusters

Xueguang Ren,[1,2,*] Enliang Wang,[3,2,†] Jiaqi Zhou,[1,2] Shaokui Jia,[1] Xing Wang,[1] Xiaorui Xue,[1] and Alexander Dorn[2]

[1]*MOE Key Laboratory for Nonequilibrium Synthesis and Modulation of Condensed Matter, School of Physics, Xi'an Jiaotong University, Xi'an 710049, China*

[2]*Max-Planck-Institut für Kernphysik, 69117 Heidelberg, Germany*

[3]*Hefei National Research Center for Physical Sciences at the Microscale and Department of Modern Physics, University of Science and Technology of China, Hefei 230026, China*

(Received 20 June 2022; revised 13 June 2023; accepted 23 October 2023; published 16 November 2023)

We report a combined experimental and theoretical study on the fragmentation dynamics following the ultrafast intermolecular Coulombic decay (ICD) in $(H_2O)_6$ water clusters upon electron impact ionization. By coincident fragment ions and electron momentum spectroscopy, we show that ICD can be initiated by inner-valence ionization of a water molecule. Our *ab initio* molecular dynamics simulations show that ICD is followed by proton transfer leading to the formation of the $(H_2O)_3 \cdot H^+ \cdots OH \cdot (H_2O)_2{}^+$ ion-radical complex. We propose a possible dissociative mechanism in which the system further dissociates into a pair of radical ions ($H_3O^+/H_5O_2{}^+$) and neutral species of water and hydrogen peroxide (H_2O_2). The calculated kinetic energy spectrum of a $H_3O^+/H_5O_2{}^+$ ion pair is in good agreement with experiment. Moreover, the present study of ICD in water provides an underlying production mechanism for the reactive oxygen species of H_2O_2 which is not considered previously in the radiolysis processes of water.

DOI: 10.1103/PhysRevA.108.052814

I. INTRODUCTION

Radiolysis, i.e., ionization and dissociation of water, is a fundamental process that leads to the formation of various reactive particles, notably hydroxyl radicals (OH), hydrogen peroxide (H_2O_2), protonated water clusters $(H_2O)_nH^+$, and hydrated electrons [1–7]. Despite the paramount importance of these processes in chemical, biophysical, and atmospheric sciences and technologies [8,9], our understanding of the primary processes and mechanisms in water radiolysis remain incomplete. Low-energy electrons (below 100 eV) are significant in this respect as they are produced abundantly in aqueous solution penetrated by any high-energy primary radiation (x rays, γ rays, and charged and neutral particles) and can induce severe structural and chemical alterations [10–12]. Hence, it is important to understand and identify the key reactions initiated by electrons in aqueous environments. These are of great relevance in such diverse fields as waste remediation and environmental cleanup, biochemistry and atmospheric science, medical radiation therapy, and nuclear reactor technologies [8–12].

In recent years, there has been intense research on the properties of excited states in the weakly bound systems or clusters due to the possibility for opening various ultrafast energy and charge-transfer processes such as the intermolecular Coulombic decay (ICD) [13]. It is a nonlocal decay mechanism which proceeds on a femtosecond timescale [14–16] and can cause the ionization of a neighboring unit. ICD results in the emission of low-energy electrons (< 10 eV) and fragment ions (see, e.g., [17]), which could have important implications, e.g., for DNA damage [9–11]. Consequently, processes following the inner-valence ionization of water-induced ICD have been investigated in hydrated systems such as water dimer [18–20], larger water clusters [21–23], liquid water [24–26], interfaces [27], and biorelevant complexes [28,29].

In these experiments, the emission of low-energy electrons has been identified and studied in detail; however, few studies have been done analyzing the ionic and neutral species formed following ICD for water clusters larger than dimers. In the present work, we use a supersonic gas jet target with small $(H_2O)_n$ clusters where most of them contain less than $n = 10$ molecules. We study electron-collision-induced ICD and the subsequent molecular dynamics of a particular fragmentation channel which we conclude to originate from ionization of the $(H_2O)_6$ parent clusters, which is also regarded as the smallest water droplet [30]. Our experiments were carried out at the projectile energy of about 80 eV that is close to the mean energy of secondary electrons produced by ionizing radiation in water [10]. The momentum vectors and, consequently, the kinetic energies of one emitted electron and two fragment ions are measured in triple coincidence using a multiparticle coincidence momentum spectrometer (reaction microscope) combined with a photoemission electron source [31–33]. We perform *ab initio* molecular dynamics (AIMD) simulations of the doubly charged water clusters using the Car-Parrinello

*renxueguang@xjtu.edu.cn
†elwang@ustc.edu.cn

molecular dynamics (CPMD) method [34] that allow us to obtain a detailed picture of the molecular rearrangement following ICD and to elucidate the chemical processes in aqueous solution.

II. EXPERIMENTAL METHODS

The experiment was performed using a multiparticle coincidence momentum spectrometer (reaction microscope) combined with a photoemission electron source [31–33]. Here, a pulsed electron beam is crossed with a gas jet consisting of water vapor. The water clusters are generated in a supersonic expansion of water vapor with a carrier gas of helium (1.0 bar pressure). The water vapor is provided from a liquid reservoir which is heated to a temperature of about 80 °C. The gas expands into vacuum from a nozzle orifice with a higher temperature of about 100 °C to avoid gas condensation. Under the present conditions, small sized water clusters are expected to be produced, i.e., $n < 10$ for $(H_2O)_n$ [35,36].

Experimental data for clusters were recorded using an electron-ion-ion triple-coincidence method in which the results for ionization of monomers were also obtained simultaneously. The charged fragments (electrons as well as ions) are extracted by means of a homogeneous electric field 0.9 V/cm and magnetic field (6.9 G) and projected onto two position- and time-sensitive multihit detectors. The momentum vectors of the emitted electrons and ions are determined by the impact positions on the detectors together with the corresponding times of flight. Ions originating from a Coulomb explosion have significantly higher momentum than the electrons observed and require higher fields for efficient detection. Thereby, after 400 ns when the electrons have reached the detector the electric extraction field is ramped up to 20 V/cm for extraction of the fragment ions.

III. MOLECULAR DYNAMICS CALCULATION

Our *ab initio* molecular dynamics simulations were carried out using the CPMD algorithm [34] in which the molecular orbitals are propagated together with the nuclear degrees of freedom. The calculations were performed with the BLYP functional in the local spin density approximation. A plane-wave basis with energy cutoff of 70 Ry is used and the core electrons are replaced by pseudopotentials of the standard Troullier-Martins form [37]. The equilibrium geometry of the neutral water cluster was first optimized and then a thermal equilibration run was performed by a Nosé-Hoover chain at a temperature of 50 K. The initial atomic configurations (positions and velocities) for AIMD simulations were taken every 2.4 fs after a long equilibration run (5 ps). The Franck-Condon picture was adopted where the dynamical simulation was started from the obtained initial configurations with two electrons being ionized from the outermost orbital of the cluster. In the simulation, a time step of 2 a.u. and a cubic box of size $L = 40$ a.u. were used. Considering the small energy difference between the singlet and triplet states (0.82 eV) and the large vibrational degrees of freedom of $(H_2O)_6$ ($3n-3=51$), the influence from the energy difference between the singlet and triplet states is negligible, and only the singlet state is considered in the simulations.

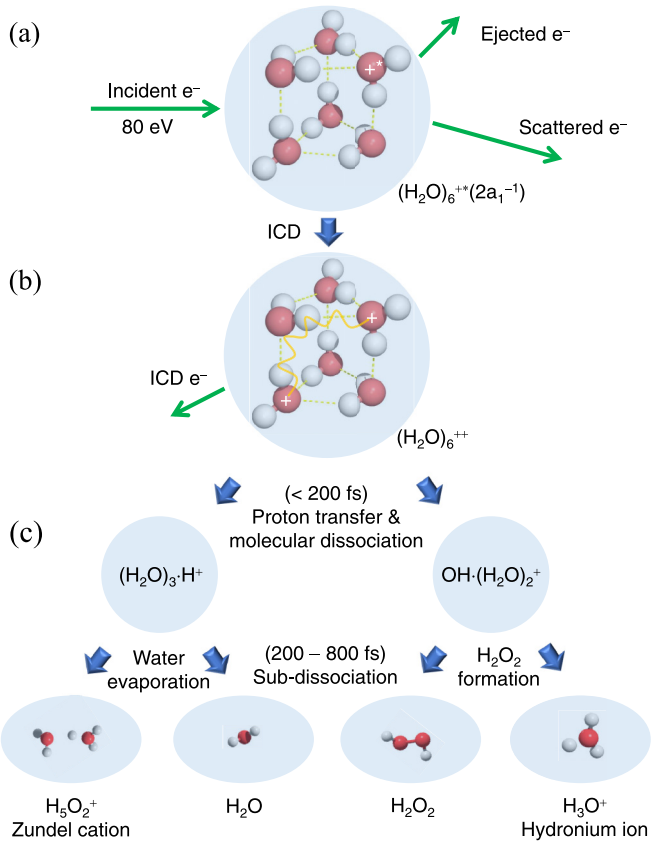

FIG. 1. Illustration of ICD in $(H_2O)_6$ water hexamer upon electron irradiation. An electron from the inner-valence shell of one H_2O molecule is ejected by electron impact (a) and then the energy released by deexcitation at this site is transferred to the neighboring site from where a second, low-energy electron is emitted (b). After ICD, the doubly charged water clusters undergo significant molecular rearrangements involving, in particular, ultrafast proton transfers and lead to the formation of specific reactive oxygen species (c).

IV. RESULTS AND DISCUSSIONS

In our experiment, we consider an electron-collision-induced reaction in the $(H_2O)_6$ water hexamer which can be expressed as

$$e^- + (H_2O)_6 \xrightarrow[\text{ionization}]{\text{inner-valence}} [H_2O]_6^+\left(2a_1^{-1}\right) + 2e^-, \quad (1)$$

$$[H_2O]_6^+\left(2a_1^{-1}\right) \xrightarrow{\text{ICD}} [H_2O]_6^{2+}\left(1b_1^{-1}; 1b_1^{-1}\right) + e^-_{\text{ICD}} \quad (2)$$

As can be seen in Fig. 1(a), the process is initiated by removal of an electron from the $2a_1$ inner-valence shell of one water molecule [Eq. (1)]. The ionized and excited system relaxes as an electron from a higher level fills the vacancy and the released energy is transferred to a neighboring water molecule which is in turn ionized through the emission of a low-energy ICD electron [Eq. (2)], as shown in Fig. 1(b). Subsequently, the doubly charged water clusters can undergo complex rearrangement and fragmentation leading to the formation of specific neutral and charged species in Fig. 1(c). It should be mentioned that ICD [Eq. (2)] competes with fast proton transfer, which according to Richter *et al.* [22], will lead to closure of the ICD channel after a few femtoseconds and to

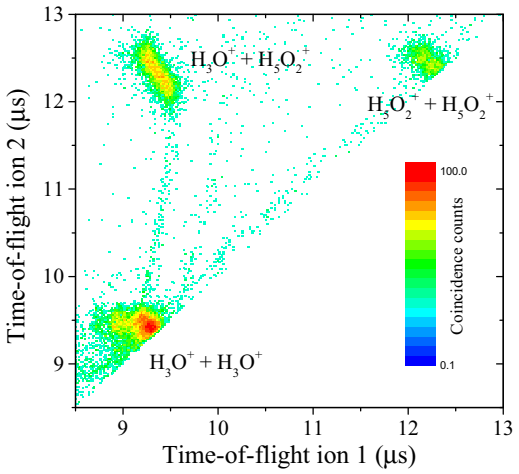

FIG. 2. Experimental time-correlation map between two fragment ions by plotting time of flight of the second ion against the first one. The intensity is color-coded on a logarithmic scale.

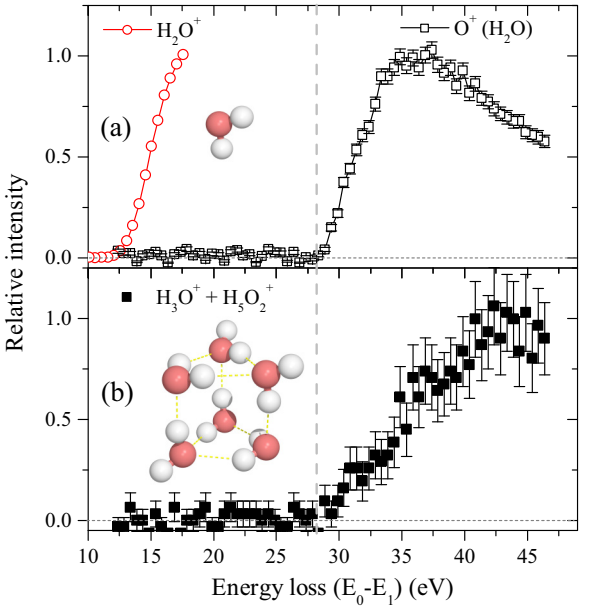

FIG. 3. Measured projectile energy-loss spectra for outer- and inner-valence ionization of water monomer (a) and for the water cluster measured in coincidence with the $H_3O^+/H_5O_2^+$ ion pair (b).

the formation of a protonated species and a highly excited OH* radical. For the small water clusters discussed here the ICD efficiency is 10%–20% [22].

The measured time-correlation map of two charged species is shown in Fig. 2 where the times of flight of two ions detected in coincidence are plotted against each other. The correlated charged pairs are mainly protonated species, i.e., H_3O^+/H_3O^+, $H_3O^+/H_5O_2^+$, and $H_5O_2^+/H_5O_2^+$ channels. The broad correlation structures indicate that there are missing momenta due to the emission of neutral fragments which cannot be detected. In the following, we focus on the dynamics of the protonated $H_3O^+/H_5O_2^+$ ion pair. For these charged products the size of the initial neutral water clusters $(H_2O)_n$ is $n = 5$ or larger. Our AIMD simulations show that the cluster $(H_2O)_6$ after double ionization will end up in this ion pair and additionally evaporate a water molecule and form the reactive oxygen species H_2O_2. This will be discussed in more detail in the following section.

In order to show that ICD actually occurs on the route to the production of the $H_3O^+/H_5O_2^+$ ion pair, we recorded the kinetic energies for one outgoing electron in coincidence with the two fragment cations. The measured electrons include scattered projectiles, directly ionized electrons, and low-energy ICD electrons. An important signature of ICD is obtained from the projectile energy-loss spectrum recorded in coincidence with the $H_3O^+/H_5O_2^+$ ion pair. This spectrum is shown in Fig. 3(b) while for comparison, in Fig. 3(a) the energy-loss spectra for ionization of water monomers in the outer-valence shell (coincidence with H_2O^+) and the $2a_1$ inner-valence shell (coincidence with O^+) [38] are presented. The projectile energy loss is determined by the difference of the initial projectile energy and the scattered projectile energy where the outgoing faster electrons are generally identified as the scattered projectiles. The minimum energy leading to specific ionization products can be determined from the onsets of the measured energy-loss spectra. The thresholds of about 12.5 and 28.0 eV are obtained for formation of H_2O^+ and O^+ ions, respectively. Here, the ionization of the outer-valence $1b_1$ and $3a_1$ orbitals contribute dominantly to the stable H_2O^+ ion, while according to the literature [38] the O^+ ionic species is attributed to the $2a_1$ inner-valence ionization of water monomer. For the $H_3O^+/H_5O_2^+$ ion pair, the obtained threshold of about 28.0 eV is consistent with the $2a_1$ inner-valence ionization band [39,40].

To identify the emitted ICD electrons the low-energy part of the electron kinetic energy spectrum up to 30 eV measured in coincidence with the ion pair is shown in Fig. 4 (open

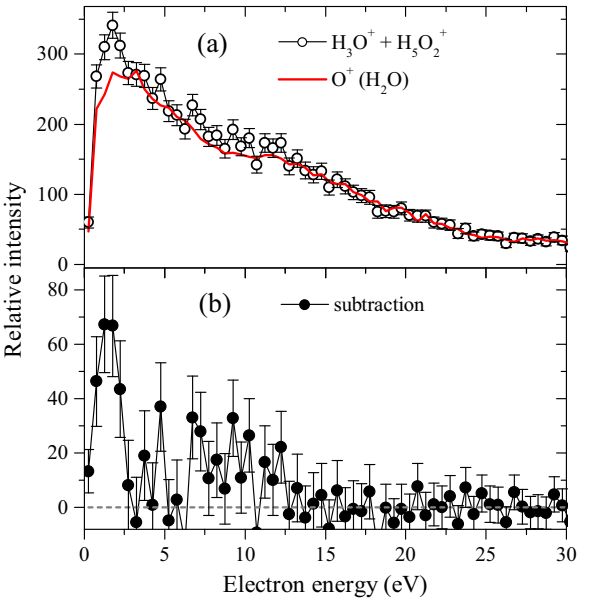

FIG. 4. Ejected electron kinetic energy distributions. (a) Spectra for inner-valence ionization of the water monomer and water cluster. (b) The difference spectrum obtained by subtracting the electron energy distribution of the water monomer from the hexamer.

circles). The emitted ICD electron as shown in Fig. 1(b) cannot be seen individually as the spectrum also contains the ejected slow electrons produced in the initial direct ionization process [see Fig. 1(a)]. Therefore, we subtract the directly ionized electron signal obtained for inner-valence ionization of water monomers which results in the formation of O^+ [see the solid line in Fig. 4(a)]. This spectrum can be considered as a reference to determine the continuous electron energy distribution due to the initial inner-valence ionization process.

The spectra for monomers and clusters are normalized to each other for energies above 15 eV where the ICD process does not contribute [22]. The difference of both spectra is shown in Fig. 4(b). It is the kinetic energy spectrum of the ICD electron which shows a peak at about 1.5 eV and a high-energy tail extending to 10–12 eV. This can be compared with the ICD electron spectra for photoionization-induced ICD in water clusters which were measured by Richter *et al.* for different mean cluster sizes [22]. Their spectra show a similar energy range but have a major intensity below 2 eV, in particular, for small mean cluster size. The agreement with our spectrum is reasonable considering that the electron detection efficiency in our experiment drops sharply below 2 eV due to the presence of a primary beam dump in the center of the electron detector which blocks low-energy electrons [41]. Another reason for the observed relative small ICD electron intensity can be that in addition to ICD, sequential ionization (SI) processes contribute to doubly charged cluster formation where two molecules in the same cluster are ionized in two consecutive collisions with the projectile. Generally, in molecular dimers its cross section can be neglected compared to the inner-valence ionization initiating ICD [41]. In the present case of water clusters the relative contribution of SI can be more significant since, firstly, the cross section is multiplied with the number of scattering centers available and, secondly, water clusters show a reduced ICD efficiency as mentioned above [22]. For water clusters ICD and SI are difficult to differentiate experimentally from the projectile energy-loss data, since both require similar energy transfer from the projectile. Nevertheless, the observed enhanced production of ICD electrons in a characteristic restricted energy range demonstrates that ICD occurs in water clusters with the formation of $H_3O^+/H_5O_2^+$ ion pairs.

To elucidate the fragmentation mechanisms of water clusters following ICD, we have performed AIMD simulations starting from the doubly charged water hexamer $(H_2O)_6^{2+}$, in which the two electrons are removed from the outermost orbital of the cluster by vertical double ionization. Such a vertical ionization picture is widely used in the AIMD simulation due to the fact that the electronic decay is faster than the molecular geometry rearrangement, thereby the ionic molecule almost keeps the same geometry as the initial neutral state. On the other hand, this assumption avoids the very time-consuming excited state calculations and, thereby, has the ability to scan the initial configurations to produce the "statistics" results in theory [42,43]. In this work, the vertical double ionization assumes that the dicationic system initially has the same geometry as the neutral, which is justified since the ICD channel is open only for less than 8 fs [22]. Moreover, SI can be considered instantaneous due to the electron scattering process occurring on a subfemtosecond timescale, which

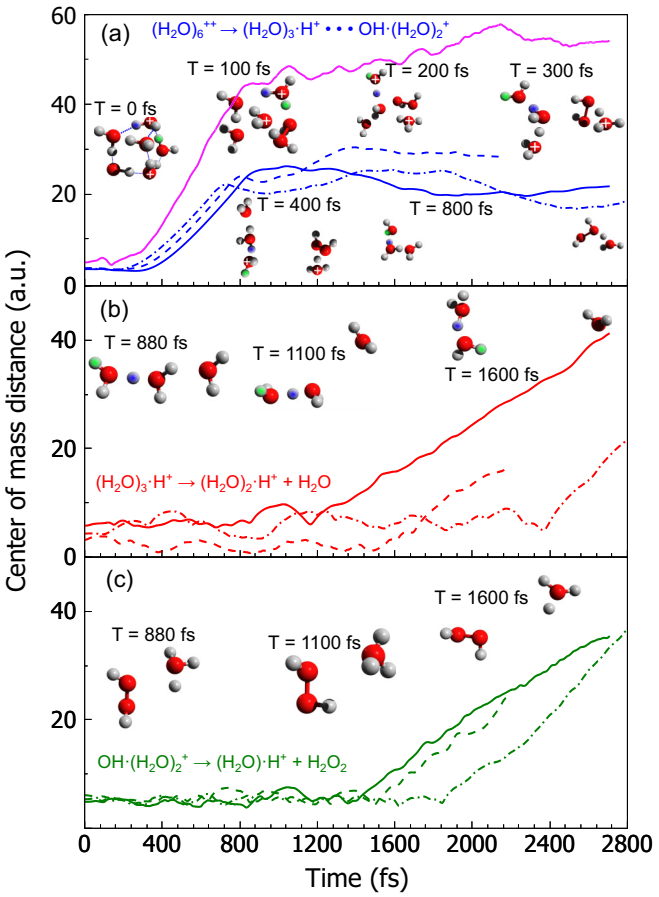

FIG. 5. Center-of-mass (c.m.) distances between different fragments as a function of time for three typical trajectories shown as solid, dashed, and dot-dashed curves, respectively. (a) For dissociation of $(H_2O)_6^{2+}$ into $(H_2O)_3 \cdot H^+$ and $OH \cdot (H_2O)_2^+$. The solid-purple line shows the c.m. between the charged fragments, $(H_2O)_2 \cdot H^+$ and $H_2O \cdot H^+$. (b) For subdissociation of $(H_2O)_3 \cdot H^+$ into $(H_2O)_2 \cdot H^+$ and H_2O, which is a neutral-dissociation process following the initial Coulomb explosion channel. (c) For subdissociation of $OH \cdot (H_2O)_2^+$ into H_3O^+ and H_2O_2.

is much faster than the nuclear vibration period, which is on the order of tens of femtoseconds. Owing to the delocalized property of the outer valence orbitals of water clusters, the two charges are distributed among the six oxygen atoms of the $(H_2O)_6^{2+}$ dication (see Appendix). For fragmentation of $(H_2O)_6^{2+}$, the final kinetic energy release can be smaller than the direct Coulomb explosion energy mainly because of the larger mean distance between the charges and also the energy transfer to the internal rotation and vibration motions of the fragments [20]. It is to be noted that the present dynamical calculations apply also for the chemical processes following photoionization-induced ICD in water clusters [21,22]. We have found a characteristic fragmentation sequence, which is presented in Fig. 5. Here the time evolution of the center-of-mass (c.m.) distances between the different fragments is shown for three typical trajectories. Also included in Fig. 5 are the cluster geometries at different times corresponding to the trajectories shown by the solid-blue, -red, and -green curves. First, we assumed an instantaneous vertical transition to the electronic ground state of the doubly charged $(H_2O)_6^{2+}$ water

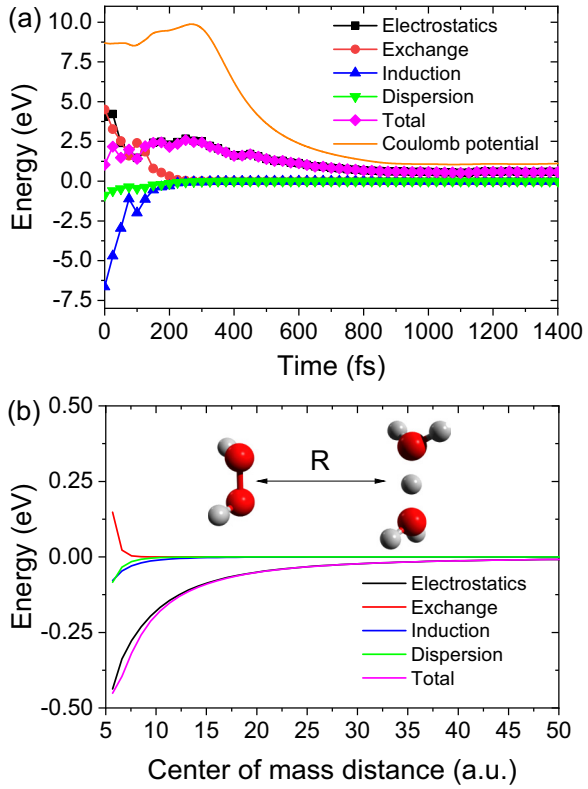

FIG. 6. (a) SAPT calculation with the aug-cc-pvdz basis set of $H_7O_3^+$ and $H_5O_3^+$ as a function of time in the range of 0–1400 fs. The Coulomb potential curve is calculated based on the point charges separated by the center-of-mass distance at the corresponding time. (b) SAPT calculation with the aug-cc-pvdz basis set of $H_5O_2^+$ and H_2O_2 as a function of the center-of-mass distance.

clusters. Afterward, a proton is transferred rapidly (< 10 fs) from one H_2O^+ to another H_2O molecule which forms the ion-radical complex of $(H_2O)_3 \cdot H^+ \cdots OH \cdot (H_2O)_2^+$:

$$(H_2O)_6^{2+} \xrightarrow[\text{transfer}]{\text{proton}} (H_2O)_3 \cdot H^+ \cdots OH \cdot (H_2O)_2^+. \quad (3)$$

The proton transfer can be seen in the consecutive cluster geometries in Fig. 5(a) where the transferred protons are marked green and blue. The white plus signs indicate the cluster constituents with dominant charges ($q \geqslant +0.5$) which were determined by Mulliken charge analysis calculated by density functional theory at the ωB97XD/aug-cc-pVTZ level [44]. As can be seen in Fig. 5(a), the system starts to separate at 200–300 fs into two ionic entities by Coulomb repulsive force. One is the protonated cluster $(H_2O)_3 \cdot H^+$, and the other is the OH radical captured cluster ion $OH \cdot (H_2O)_2^+$. After that the c.m. distance between $(H_2O)_3 \cdot H^+$ and $OH \cdot (H_2O)_2^+$ is almost linearly increasing as a function of time to about 20 a.u. ($t \sim 800$ fs) where the c.m. distance does not increase further but oscillates around about 20 a.u. [see Fig. 5(a)]. This indicates that the two-body dissociation of $(H_2O)_3 \cdot H^+$ and $OH \cdot (H_2O)_2^+$ cannot be described by the Coulomb explosion model. We perform the symmetry-adapted perturbation theory (SAPT) calculation [45–47] with the aug-cc-pVDZ basis set to calculate the interaction energy of the two dissociative species. As shown in Fig. 6(a), at large time, the electrostatic interaction dominates, which deviates from the Coulomb potential as shown by the solid black and orange curves, respectively, in Fig. 6(a) and the positive interaction energy indicates a dissociative state. Thereafter the center-of-mass distances of Fig. 5(a) are mainly determined by the heavier groups of the subspecies, i.e., $H_5O_2^+$ and H_2O_2.

At $t \sim 800$ fs, the translatory energy is converted into internal vibration and rotation of the two fragments. Consequently, further dissociation processes occur as described in Eqs. (4) and (5):

$$(H_2O)_3 \cdot H^+ \xrightarrow[\text{evaporation}]{\text{water}} (H_2O)_2H^+ + H_2O, \quad (4)$$

$$OH \cdot (H_2O)_2^+ \xrightarrow[\text{formation}]{H_2O_2} H_3O^+ + H_2O_2. \quad (5)$$

We found in the simulations that the system undergoes significant rearrangements of the structure involving particularly proton transfer leading to the formation of specific ionic and neutral fragments. The dipole moment interaction between the charged and neutral molecules plays an important role which can produce an attractive force to compensate for the Coulomb repulsion force to some extent. To analyze the interaction energy between the two heavier species, i.e.. $H_5O_2^+$ and H_2O_2, we extract the two subspecies and optimize their geometries by the B3LYP/aug-cc-pVDZ method. Then, we use the SAPT/aug-cc-pVDZ method to calculate the interaction energy of $H_5O_2^+$ and H_2O_2 as a function of the center-of-mass distance. As expected, the SAPT calculation shows a negative total interaction energy between $H_5O_2^+$ and H_2O_2 as shown in Fig. 6(b). The negative value of the total interaction energy means an attractive force between $H_5O_2^+$ and H_2O_2. Ignoring the neutral species, the internuclear distance between the charge centers of the final $H_5O_2^+$ and H_3O^+ increases almost monotonically as a function of time, while the slope is decreased at $t > 800$ fs as shown by the solid-purple curve in Fig. 5(a).

Furthermore, the $(H_2O)_3 \cdot H^+$ group starts at $t \sim 880$ fs to evaporate a neutral H_2O molecule and forms a Zundel cation $H_5O_2^+$. The $OH \cdot (H_2O)_2^+$ group yields a hydronium cation (H_3O^+) and, more interestingly, hydrogen peroxide (H_2O_2) which is a key member of reactive oxygen species in the radiolysis of water [8,48]. We note that the H_2O_2 was also observed in the energetic electron collision experiments on water ice (solid film), where the formation mechanism remains unclear [6,7]. Before evaporating neutral H_2O and H_2O_2 the internal energies of $(H_2O)_3 \cdot H^+$ and $OH \cdot (H_2O)_2^+$ are rather high leading to oscillations on c.m. distance distributions as shown in Figs. 5(b) and 5(c). The oscillations almost disappear after evaporating the neutral species as the internal energy is released in kinetic fragment energy. In our simulations, 29% trajectories terminated as $H_3O^+ + H_5O_2^+ + H_2O + H_2O_2$, which indicates the dominance of this dissociation channel.

For completeness we performed AIMD simulations for the clusters of $(H_2O)_5^{2+}$ and $(H_2O)_7^{2+}$ where chemical processes similar to $(H_2O)_6^{2+}$ are obtained except for the formations of different ion pairs, e.g., H_3O^+/H_3O^+ and $H_5O_2^+/H_5O_2^+$ ion pairs, respectively. This shows that the conclusion that the

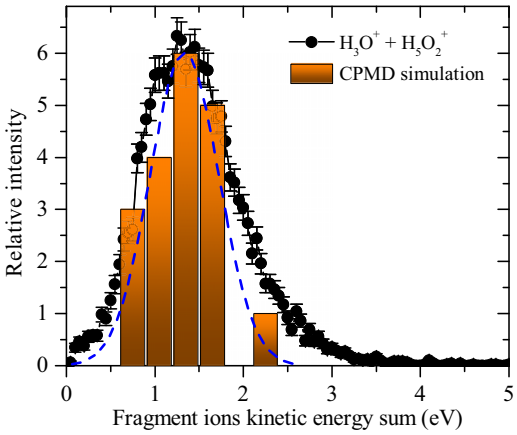

FIG. 7. Comparison of the experimental and calculated kinetic energy sum of charged fragments. The blue-dashed curve presents a Gaussian fitting of the simulation.

$H_3O^+/H_5O_2^+$ ion pair originates from the initial cluster of $(H_2O)_6$ is reasonable.

Finally, we obtain the kinetic energy sum (KES) spectrum of the $H_3O^+/H_5O_2^+$ ion pair from the AIMD simulations, which is shown in Fig. 7. For all trajectories, at the end of the simulation the c.m. distances between two charged species are larger than 15 a.u.. At this distance we take the rovibrational energy as constant and the KES can be obtained by summing the kinetic energies of two fragment ions at this instant plus the remaining Coulomb potential energy. Also included in Fig. 7 is the experimental KES, which shows a peak located at about 1.35 eV. The calculated KES is in excellent agreement with the experimental data concerning both the shape and the peak position of the spectrum. The present dynamical calculations are thereby justified.

V. CONCLUSIONS

In summary, our study of ICD in water clusters using fragment ion and electron coincident momentum spectroscopy, accompanied by AIMD simulations, reveals the details of ionization and fragmentation dynamics upon inner-valence ionization in aqueous solution initiated by electrons (80 eV). The occurrence of the ICD process is proven by determining the initial state of ICD as a $2a_1$ inner-valence vacancy in water from the projectile energy loss and a signature of secondary low-energy ICD electrons in coincidence with two energetic cations.

The chemical processes of water clusters following ICD were interpreted with the help of AIMD simulations. Our study shows that after ICD the system undergoes significant rearrangement involving particularly proton transfer and Coulomb explosion (<200 fs) as well as subdissociation (<800 fs) leading to the formation of specific reactive oxygen species. These are a pair of protonated water clusters and neutral species of a water molecule and H_2O_2. Despite the complexity of the fragmentation reaction the AIMD simulations show excellent agreement with the experimental results of the kinetic energy sum of the $H_3O^+/H_5O_2^+$ ion pair. For the formation of hydrogen peroxide, various reaction channels

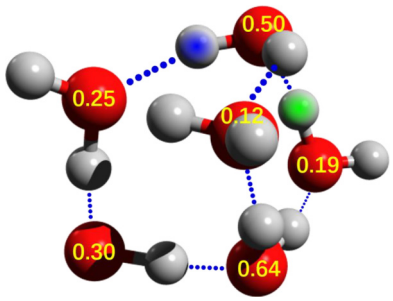

FIG. 8. The calculated charge distribution of $(H_2O)_6^{2+}$ by removal of two outermost electrons from the clusters.

have been revealed, e.g., from an irradiation of water ice by energetic electrons [6,7], water clusters of an oxygen radical anion upon photodetachment [49], and oxidation of water microdroplets [50]. The present observation offers a possible production mechanism for H_2O_2 occurring in water radiolysis, which was not considered previously. It also differs from the mechanisms due to reactions of the OH radicals within the energetic ionizing particle track [8,51,52] by the fact that ICD relies on the creation of an inner-valence vacancy in aqueous environment and leads to two radical cations neighboring each other. Moreover, in simulations on the larger cluster of $(H_2O)_7$, we have also observed H_2O_2 formation, which indicates that $(H_2O)_6$ is not unique in producing H_2O_2. These results enable a deeper and more complete understanding of water radiolysis at the molecular level, which can have important implications for different fields like cell functions [53–55], radiosensitizers [56,57], and H_2O_2-induced DNA damage [58–60]. On the grounds of our findings, we anticipate that the present observation may occur generally in a wide variety of hydrated systems for inducing different chemical reactions and can also be initiated by other intermolecular decay mechanisms like electron-transfer-mediated decay [61–63]. Future studies on more complex systems or using ultrashort pulses from free-electron lasers and high harmonics sources for time-resolved experiments [1–3,64–66] are expected to shed more light on the formation time

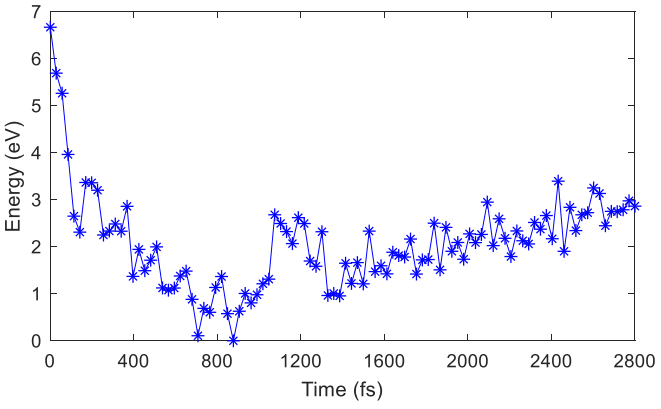

FIG. 9. The potential energy of $(H_2O)_6^{2+}$ as a function of the time.

and dynamical details of H_2O_2 and ICD-induced chemical processes in condensed media.

ACKNOWLEDGMENTS

This work was jointly supported by the National Natural Science Foundation of China under Grants No. 92261201, No. 11974272, and No. 12325406; and Shaanxi Fundamental Science Research Project for Mathematics and Physics under Grant No. 22JSY022. E.W. is supported by the Strategic Priority Research Program of Chinese Academy of Sciences under Grant No. XDB34020000 and a fellowship from the Alexander von Humboldt Foundation. X.R. is grateful for support from the Shaanxi Province Natural Science Fundamental Research Project under Grant No. 2023JC-XJ-03.

APPENDIX: CHARGE DISTRIBUTION AND POTENTIAL ENERGY OF $(H_2O)_6^{2+}$

1. Charge distribution of $(H_2O)_6^{2+}$

The calculated Mulliken charge of $(H_2O)_6^{2+}$ by density functional theory using the ωB97XD functional with the aug-cc-pVTZ basis set is shown in Fig. 8. The two charges in the cluster are distributed among six oxygen atoms.

2. Potential energy of $(H_2O)_6^{2+}$

The potential energy of $(H_2O)_6^{2+}$ as a function of the time is shown in Fig. 9. The trajectory corresponds to the solid blue curves in Fig. 5. At each point, the geometry is extracted from the *ab initio* simulation and the potential energy is calculated by the B3LYP/Aug-cc-pVDZ method.

[1] Z.-H. Loh, G. Doumy, C. Arnold, L. Kjellsson, S. H. Southworth, A. Al Haddad, Y. Kumagai, M.-F. Tu, P. J. Ho, A. M. March, R. D. Schaller, M. S. Bin Mohd Yusof, T. Debnath, M. Simon, R. Welsch, L. Inhester, K. Khalili, K. Nanda, A. I. Krylov, S. Moeller *et al.*, Observation of the fastest chemical processes in the radiolysis of water, Science **367**, 179 (2020).

[2] V. Svoboda, R. Michiels, A. C. LaForge, J. Med, F. Stienkemeier, P. Slavíček, and H. J. Wörner, Real-time observation of water radiolysis and hydrated electron formation induced by extreme-ultraviolet pulses, Sci. Adv. **6**, eaaz0385 (2020).

[3] M.-F. Lin, N. Singh, S. Liang, M. Mo, J. P. F. Nunes, K. Ledbetter, J. Yang, M. Kozina, S. Weathersby, X. Shen, A. A. Cordones, T. J. A. Wolf, C. D. Pemmaraju, M. Ihme, and X. J. Wang, Imaging the short-lived hydroxyl-hydronium pair in ionized liquid water, Science **374**, 92 (2021).

[4] J. M. Herbert and M. P. Coons, The hydrated electron, Annu. Rev. Phys. Chem. **68**, 447 (2017).

[5] E. Alizadeh and L. Sanche, Precursors of solvated electrons in radiobiological physics and chemistry, Chem. Rev. **112**, 5578 (2012).

[6] W. Zheng, D. Jewitt, and R. I. Kaiser, Temperature dependence of the formation of hydrogen, oxygen, and hydrogen peroxide in electron-irradiated crystalline water ice, Astrophys. J. **648**, 753 (2006).

[7] W. Zheng, D. Jewitt, and R. I. Kaiser, Formation of hydrogen, oxygen, and hydrogen peroxide in electron-irradiated crystalline water ice, Astrophys. J. **639**, 534 (2006).

[8] B. C. Garrett, D. A. Dixon, D. M. Camaioni, D. M. Chipman, M. A. Johnson, C. D. Jonah, G. A. Kimmel, J. H. Miller, T. N. Rescigno, P. J. Rossky, S. S. Xantheas, S. D. Colson, A. H. Laufer, D. Ray, P. F. Barbara, D. M. Bartels, K. H. Becker, K. H. Bowen, S. E. Bradforth, I. Carmichael *et al.*, Role of water in electron-initiated processes and radical chemistry: Issues and scientific advances, Chem. Rev. **105**, 355 (2005).

[9] E. Alizadeh, T. M. Orlando, and L. Sanche, Biomolecular damage induced by ionizing radiation: The direct and indirect effects of low-energy electrons on DNA, Annu. Rev. Phys. Chem. **66**, 379 (2015).

[10] S. M. Pimblott and J. A. LaVerne, Production of low-energy electrons by ionizing radiation, Radiat. Phys. Chem. **76**, 1244 (2007).

[11] M. A. Huels, B. Boudaiffa, P. Cloutier, D. Hunting, and L. Sanche, Single, double, and multiple double strand breaks induced in DNA by 3−100 eV electrons, J. Am. Chem. Soc. **125**, 4467 (2003).

[12] J. Zhou, S. Jia, X. Hu, E. Wang, X. Xue, Y. Wu, J. Wang, A. Dorn, and X. Ren, Intermolecular charge transfer induced fragmentation of formic acid dimers, Phys. Rev. Lett. **130**, 233001 (2023).

[13] L. S. Cederbaum, J. Zobeley, and F. Tarantelli, Giant intermolecular decay and fragmentation of clusters, Phys. Rev. Lett. **79**, 4778 (1997).

[14] G. Öhrwall, M. Tchaplyguine, M. Lundwall, R. Feifel, H. Bergersen, T. Rander, A. Lindblad, J. Schulz, S. Peredkov, S. Barth, S. Marburger, U. Hergenhahn, S. Svensson, and O. Björneholm, Femtosecond interatomic Coulombic decay in free neon clusters: Large lifetime differences between surface and bulk, Phys. Rev. Lett. **93**, 173401 (2004).

[15] K. Schnorr, A. Senftleben, M. Kurka, A. Rudenko, L. Foucar, G. Schmid, A. Broska, T. Pfeifer, K. Meyer, D. Anielski, R. Boll, D. Rolles, M. Kübel, M. F. Kling, Y. H. Jiang, S. Mondal, T. Tachibana, K. Ueda, T. Marchenko, M. Simon *et al.*, Time-resolved measurement of interatomic Coulombic decay in Ne_2, Phys. Rev. Lett. **111**, 093402 (2013).

[16] F. Trinter, J. B. Williams, M. Weller, M. Waitz, M. Pitzer, J. Voigtsberger, C. Schober, G. Kastirke, C. Müller, C. Goihl, P. Burzynski, F. Wiegandt, T. Bauer, R. Wallauer, H. Sann, A. Kalinin, L. P. H. Schmidt, M. Schöffler, N. Sisourat, and T. Jahnke, Evolution of interatomic Coulombic decay in the time domain, Phys. Rev. Lett. **111**, 093401 (2013).

[17] T. Jahnke, U. Hergenhahn, B. Winter, R. Dörner, U. Frühling, P. V. Demekhin, K. Gokhberg, L. S. Cederbaum, A. Ehresmann, A. Knie, and A. Dreuw, Interatomic and intermolecular Coulombic decay, Chem. Rev. **120**, 11295 (2020).

[18] T. Jahnke, H. Sann, T. Havermeier, K. Kreidi, C. Stuck, M. Meckel, M. Schöffler, N. Neumann, R. Wallauer, S. Voss, A. Czasch, O. Jagutzki, A. Malakzadeh, F. Afaneh, T. Weber,

H. Schmidt-Böcking, and R. Dörner, Ultrafast energy transfer between water molecules, Nat. Phys. **6**, 139 (2010).

[19] S. D. Stoychev, A. I. Kuleff, and L. S. Cederbaum, On the intermolecular Coulombic decay of singly and doubly ionized states of water dimer, J. Chem. Phys. **133**, 154307 (2010).

[20] O. Vendrell, S. D. Stoychev, and L. S. Cederbaum, Generation of highly damaging H_2O^+ radicals by inner valence shell ionization of water, ChemPhysChem **11**, 1006 (2010).

[21] M. Mucke, M. Braune, S. Barth, M. Forstel, T. Lischke, V. Ulrich, T. Arion, U. Becker, A. Bradshaw, and U. Hergenhahn, A hitherto unrecognized source of low-energy electrons in water, Nat. Phys. **6**, 143 (2010).

[22] C. Richter, D. Hollas, C.-M. Saak, M. Förstel, T. Miteva, M. Mucke, O. Björneholm, N. Sisourat, P. Slavíček, and U. Hergenhahn, Competition between proton transfer and intermolecular Coulombic decay in water, Nat. Commun. **9**, 4988 (2018).

[23] I. B. Müller and L. S. Cederbaum, Ionization and double ionization of small water clusters, J. Chem. Phys. **125**, 204305 (2006).

[24] S. Thürmer, M. Oncak, N. Ottosson, R. Seidel, U. Hergenhahn, S. E. Bradforth, P. Slavicek, and B. Winter, On the nature and origin of dicationic, charge-separated species formed in liquid water on x-ray irradiation, Nat. Chem. **5**, 590 (2013).

[25] E. F. Aziz, N. Ottosson, M. Faubel, I. V. Hertel, and B. Winter, Interaction between liquid water and hydroxide revealed by core-hole de-excitation, Nature (London) **455**, 89 (2008).

[26] P. Zhang, C. Perry, T. T. Luu, D. Matselyukh, and H. J. Wörner, Intermolecular Coulombic decay in liquid water, Phys. Rev. Lett. **128**, 133001 (2022).

[27] G. A. Grieves and T. M. Orlando, Intermolecular Coulomb decay at weakly coupled heterogeneous interfaces, Phys. Rev. Lett. **107**, 016104 (2011).

[28] X. Ren, E. Wang, A. D. Skitnevskaya, A. B. Trofimov, K. Gokhberg, and A. Dorn, Experimental evidence for ultrafast intermolecular relaxation processes in hydrated biomolecules, Nat. Phys. **14**, 1062 (2018).

[29] S. D. Stoychev, A. I. Kuleff, and L. S. Cederbaum, Intermolecular Coulombic decay in small biochemically relevant hydrogen-bonded systems, J. Am. Chem. Soc. **133**, 6817 (2011).

[30] J. O. Richardson, C. Pérez, S. Lobsiger, A. A. Reid, B. Temelso, G. C. Shields, Z. Kisiel, D. J. Wales, B. H. Pate, and S. C. Althorpe, Concerted hydrogen-bond breaking by quantum tunneling in the water hexamer prism, Science **351**, 1310 (2016).

[31] J. Ullrich, R. Moshammer, A. Dorn, R. Dörner, L. P. H. Schmidt, and H. Schmidt-Böcking, Recoil-ion and electron momentum spectroscopy: Reaction-microscopes, Rep. Prog. Phys. **66**, 1463 (2003).

[32] X. Ren, J. Zhou, E. Wang, T. Yang, Z. Xu, N. Sisourat, T. Pfeifer, and A. Dorn, Ultrafast energy transfer between π-stacked aromatic rings upon inner-valence ionization, Nat. Chem. **14**, 232 (2022).

[33] S. Jia, J. Zhou, X. Wang, X. Xue, X. Hao, Q. Zeng, Y. Zhao, Z. Xu, A. Dorn, and X. Ren, Cold-target electron-ion-coincidence momentum-spectroscopy study of electron-impact single and double ionization of N_2 and O_2 molecules, Phys. Rev. A **107**, 032819 (2023).

[34] R. Car and M. Parrinello, Unified approach for molecular dynamics and density-functional theory, Phys. Rev. Lett. **55**, 2471 (1985).

[35] L. Adoui, A. Cassimi, B. Gervais, J.-P. Grandin, L. Guillaume, R. Maisonny, S. Legendre, M. Tarisien, P. López-Tarifa, M.-F. Politis, M.-A. H. du Penhoat, R. Vuilleumier, M.-P. Gaigeot, I. Tavernelli, M. Alcamí, and F. Martín, Ionization and fragmentation of water clusters by fast highly charged ions, J. Phys. B: At., Mol. Opt. Phys. **42**, 075101 (2009).

[36] C. Bobbert, S. Schütte, C. Steinbach, and U. Buck, Fragmentation and reliable size distributions of large ammonia and water clusters, Eur. Phys. J. D **19**, 183 (2002).

[37] N. Troullier and J. L. Martins, Efficient pseudopotentials for plane-wave calculations. II. Operators for fast iterative diagonalization, Phys. Rev. B **43**, 8861 (1991).

[38] K. H. Tan, C. E. Brion, P. E. van der Leeuw, and M. J. van der Wiel, Absolute oscillator strengths (10-60 eV) for the photoabsorption, photoionisation and fragmentation of H_2O, Chem. Phys. **29**, 299 (1978).

[39] S. Barth, M. Ončák, V. Ulrich, M. Mucke, T. Lischke, P. Slavíček, and U. Hergenhahn, Valence ionization of water clusters: From isolated molecules to bulk, J. Phys. Chem. A **113**, 13519 (2009).

[40] C. G. Ning, B. Hajgató, Y. R. Huang, S. F. Zhang, K. Liu, Z. H. Luo, S. Knippenberg, J. K. Deng, and M. S. Deleuze, High resolution electron momentum spectroscopy of the valence orbitals of water, Chem. Phys. **343**, 19 (2008).

[41] X. Ren, E. Jabbour Al Maalouf, A. Dorn, and S. Denifl, Direct evidence of two interatomic relaxation mechanisms in argon dimers ionized by electron impact, Nat. Commun. **7**, 11093 (2016).

[42] N. G. Kling, S. Díaz-Tendero, R. Obaid, M. R. Disla, H. Xiong, M. Sundberg, S. D. Khosravi, M. Davino, P. Drach, A. M. Carroll, T. Osipov, F. Martín, and N. Berrah, Time-resolved molecular dynamics of single and double hydrogen migration in ethanol, Nat. Commun. **10**, 2813 (2019).

[43] E. Erdmann, M. Łabuda, N. F. Aguirre, S. Díaz-Tendero, and M. Alcamí, Furan fragmentation in the gas phase: New insights from statistical and molecular dynamics calculations, J. Phys. Chem. A **122**, 4153 (2018).

[44] M. J. Frisch, G. W. Trucks, H. B. Schlegel, G. E. Scuseria, M. A. Robb, J. R. Cheeseman, G. Scalmani, V. Barone, G. A. Petersson, H. Nakatsuji, X. Li, M. Caricato, A. V. Marenich, J. Bloino, B. G. Janesko, R. Gomperts, B. Mennucci, H. P. Hratchian, J. V. Ortiz, A. F. Izmaylov *et al.*, Gaussian16 revision A.03 (Gaussian Inc. Wallingford CT, 2016).

[45] D. G. A. Smith, L. A. Burns, A. C. Simmonett, R. M. Parrish, M. C. Schieber, R. Galvelis, P. Kraus, H. Kruse, R. Di Remigio, A. Alenaizan, A. M. James, S. Lehtola, J. P. Misiewicz, M. Scheurer, R. A. Shaw, J. B. Schriber, Y. Xie, Z. L. Glick, D. A. Sirianni, J. S. OâBrien *et al.*, PSI4 1.4: Open-source software for high-throughput quantum chemistry, J. Chem. Phys. **152**, 184108 (2020).

[46] B. Jeziorski, R. Moszynski, and K. Szalewicz, Perturbation theory approach to intermolecular potential energy surfaces of van der Waals complexes, Chem. Rev. **94**, 1887 (1994).

[47] T. M. Parker, L. A. Burns, R. M. Parrish, A. G. Ryno, and C. D. Sherrill, Levels of symmetry adapted perturbation theory

(SAPT). I. Efficiency and performance for interaction energies, J. Chem. Phys. **140**, 094106 (2014).

[48] B. Yang, Y. Chen, and J. Shi, Reactive oxygen species (ROS)-based nanomedicine, Chem. Rev. **119**, 4881 (2019).

[49] H. Tachikawa, Formation of hydrogen peroxide from $O^-(H_2O)_n$ clusters, J. Phys. Chem. A **125**, 4598 (2021).

[50] J. K. Lee, H. S. Han, S. Chaikasetsin, D. P. Marron, R. M. Waymouth, F. B. Prinz, and R. N. Zare, Condensing water vapor to droplets generates hydrogen peroxide, Proc. Natl. Acad. Sci. USA **117**, 30934 (2020).

[51] V. Wasselin-Trupin, G. Baldacchino, S. Bouffard, and B. Hickel, Hydrogen peroxide yields in water radiolysis by high-energy ion beams at constant LET, Radiat. Phys. Chem. **65**, 53 (2002).

[52] K. Iwamatsu, S. Sundin, and J. A. LaVerne, Hydrogen peroxide kinetics in water radiolysis, Radiat. Phys. Chem. **145**, 207 (2018).

[53] T. J. Jönsson, L. C. Johnson, and W. T. Lowther, Structure of the sulphiredoxin–peroxiredoxin complex reveals an essential repair embrace, Nature (London) **451**, 98 (2008).

[54] T. Finkel and N. J. Holbrook, Oxidants, oxidative stress and the biology of ageing, Nature (London) **408**, 239 (2000).

[55] M. Sundaresan, Z.-X. Yu, V. J. Ferrans, K. Irani, and T. Finkel, Requirement for generation of H_2O_2 for platelet-derived growth factor signal transduction, Science **270**, 296 (1995).

[56] H. Wang, X. Mu, H. He, and X.-D. Zhang, Cancer radiosensitizers, Trends Pharmacol. Sci. **39**, 24 (2018).

[57] S. Kariya, K. Sawada, T. Kobayashi, T. Karashima, T. Shuin, A. Nishioka, and Y. Ogawa, Combination treatment of hydrogen peroxide and x-rays induces apoptosis in human prostate cancer PC-3 cells, Int. J. Radiat. Oncol. Biol. Phys. **75**, 449 (2009).

[58] C. von. Sonntag, *Free-Radical-Induced DNA Damage and its Repair: A Chemical Perspective* (Springer, New York, 2011).

[59] M. López-Lázaro, Dual role of hydrogen peroxide in cancer: Possible relevance to cancer chemoprevention and therapy, Cancer Lett. **252**, 1 (2007).

[60] G. Calabrese, E. Peker, P. S. Amponsah, M. N. Hoehne, T. Riemer, M. Mai, G. P. Bienert, M. Deponte, B. Morgan, and J. Riemer, Hyperoxidation of mitochondrial peroxiredoxin limits H_2O_2-induced cell death in yeast, EMBO J. **38**, e101552 (2019).

[61] P. Slavíček, N. V. Kryzhevoi, E. F. Aziz, and B. Winter, Relaxation processes in aqueous systems upon x-ray ionization: Entanglement of electronic and nuclear dynamics, J. Phys. Chem. Lett. **7**, 234 (2016).

[62] V. Stumpf, K. Gokhberg, and L. S. Cederbaum, The role of metal ions in x-ray-induced photochemistry, Nat. Chem. **8**, 237 (2016).

[63] I. Unger, R. Seidel, S. Thürmer, M. N. Pohl, E. F. Aziz, L. S. Cederbaum, E. Muchová, P. Slavíček, B. Winter, and N. V. Kryzhevoi, Observation of electron-transfer-mediated decay in aqueous solution, Nat. Chem. **9**, 708 (2017).

[64] T. Jahnke, R. Guillemin, L. Inhester, S.-K. Son, G. Kastirke, M. Ilchen, J. Rist, D. Trabert, N. Melzer, N. Anders, T. Mazza, R. Boll, A. De Fanis, V. Music, T. Weber, M. Weller, S. Eckart, K. Fehre, S. Grundmann, A. Hartung *et al.*, Inner-shell-ionization-induced femtosecond structural dynamics of water molecules imaged at an x-ray free-electron laser, Phys. Rev. X **11**, 041044 (2021).

[65] M. Zhang, Z. Guo, X. Mi, Z. Li, and Y. Liu, Ultrafast imaging of molecular dynamics using ultrafast low-frequency lasers, x-ray free electron lasers, and electron pulses, J. Phys. Chem. Lett. **13**, 1668 (2022).

[66] Z. Wang, X. Hu, X. Xue, S. Zhou, X. Li, Y. Yang, J. Zhou, Z. Shu, B. Zhao, X. Yu, M. Gong, Z. Wang, P. Ma, Y. Wu, X. Chen, J. Wang, X. Ren, C. Wang, and D. Ding, Directly imaging excited state-resolved transient structures of water induced by valence and inner-shell ionisation, Nat. Commun. **14**, 5420 (2023).